Prospects of Using Tidal Tomography to Constrain Ganymede's Interior

Rovira-Navarro, M.; Matsuyama, I.; Dirkx, D.; Berne, A.; Calliess, D.; Fayolle, S.

DOI
10.1029/2025GL114708

Publication date
2025

Document Version
Final published version

Published in
Geophysical Research Letters

Geophysical Research Letters

RESEARCH LETTER
10.1029/2025GL114708

Prospects of Using Tidal Tomography to Constrain Ganymede's Interior

M. Rovira-Navarro[1], I. Matsuyama[2], D. Dirkx[1], A. Berne[3], D. Calliess[1], and S. Fayolle[1,4]

[1]Faculty of Aerospace Engineering, TU Delft, Delft, The Netherlands, [2]Lunar and Planetary Laboratory, University of Arizona, Tucson, AZ, USA, [3]Division of Geological and Planetary Sciences, California Institute of Technology, Pasadena, CA, USA, [4]European Space Research and Technology Centre, ESA, Noordwijk, The Netherlands

Key Points:

- We investigate the potential of using measurements of Ganymede's tides to constrain lateral structure in its interior
- $l = 2$ and $l = 3$ tidal observations can reveal an equator/pole and hemispherical dichotomy, respectively
- Future gravity inversions should consider a more complex tidal response able to capture the role of lateral heterogenities

Supporting Information:

Supporting Information may be found in the online version of this article.

Correspondence to:

M. Rovira-Navarro,
m.roviranavarro@tudelft.nl

Citation:

Rovira-Navarro, M., Matsuyama, I., Dirkx, D., Berne, A., Calliess, D., & Fayolle, S. (2025). Prospects of using tidal tomography to constrain Ganymede's interior. *Geophysical Research Letters*, *52*, e2025GL114708. https://doi.org/10.1029/2025GL114708

Received 13 JAN 2025
Accepted 14 APR 2025

Author Contributions:

Conceptualization: M. Rovira-Navarro, I. Matsuyama
Formal analysis: M. Rovira-Navarro, D. Dirkx, A. Berne, D. Calliess
Investigation: M. Rovira-Navarro, A. Berne, D. Calliess
Methodology: M. Rovira-Navarro, A. Berne
Software: M. Rovira-Navarro, D. Dirkx
Validation: A. Berne
Visualization: M. Rovira-Navarro
Writing – original draft: M. Rovira-Navarro
Writing – review & editing: M. Rovira-Navarro, I. Matsuyama, D. Dirkx, A. Berne, S. Fayolle

Abstract Juice (JUpiter ICy moons Explorer) 3GM Radio Science Experiment will map the gravitational field of Ganymede with unprecedented accuracy and measure tidally-induced variations. These measurements will allow the characterization of its putative ocean and may resolve lateral variations in internal structure. Lateral variations cause an additional tidal signal that depends on their wavelength and amplitude. We show that shell thickness variations of $10 - 100\%$ the mean thickness produce an additional tidal signal $\sim 10^2 - 10^3$ times smaller than the main tidal signal, detectable given the accuracy of Juice. Using a Bayesian framework, we show that measuring differences between k_{20} and k_{22} constrain equator to pole shell thickness differences. Also measuring the degree-3 spherical harmonic signal due to degree 2 forcing constrain degree-1 and degree-3 structure. This demonstrates tidal tomography's potential to map three dimensional structure and supports its consideration for future missions.

Plain Language Summary In 2034, the Juice (JUpiter ICy moons Explorer) spacecraft is set to enter orbit around Jupiter's moon Ganymede. Measurements of its tidal deformation will allow confirmation of the existence of a subsurface water ocean and determine the thickness of its icy crust. Juice's highly accurate tidal measurements will make it possible to map lateral variations in Ganymede's ice shell thickness using tidal tomography, a technique previously only used on Earth. Inferring the presence of these variations offers a window into the satellite's internal dynamics (e.g., ocean circulation and the long-term evolution of the ice shell).

1. Introduction

Tidal observations have constrained the interior properties of several planetary bodies beyond Earth, including Mercury (e.g., Padovan et al., 2014), Venus (e.g., Konopliv & Yoder, 1996), the Moon (e.g., Goossens, Matsuyama, et al., 2024; Williams et al., 2014), Mars (e.g., Pou et al., 2022; Yoder et al., 2003), Titan (e.g., Durante et al., 2019; Goossens, van Noort et al., 2024; Iess et al., 2012) and Io (Park et al., 2024). If all goes well, Ganymede will be soon added to this list.

After a successful launch in 2023, the JUpiter ICy moons Explorer (Juice) mission is on its way to Jupiter, where it will investigate the habitability of the Galilean moons with special emphasis on Ganymede (Grasset et al., 2013). In 2034, Juice will enter orbit around Ganymede, starting with a 150-day long high-altitude phase and culminating with a 130-day long 490 km (GCO-500) and a 30-day long 200 km (GCO-200) circular orbit phase (Boutonnet et al., 2024). This will allow the characterization of Ganymede's ice shell and putative subsurface ocean using, among other observations, measurements of tidal deformation over the course of the moon's 7 day elliptical orbit around Jupiter (e.g., Kivelson et al., 2002; Saur et al., 2015; Van Hoolst et al., 2024). During Juice's orbital phase, two instruments will measure Ganymede's tides: GALA (Ganymede Laser Altimeter) will directly measure tidally-induced radial displacements of the outer surface (Hussmann et al., 2019) and the 3GM Radio Science Experiment (Geodesy and Geophysics of Jupiter and the Galilean Moons) will measure the impact of Ganymede's tides on the satellite's time varying gravity field via subtle changes in Juice's orbit (Cappuccio et al., 2020).

With the notable exception of A et al. (2014), previous studies have focused on exploiting tidal observations to constrain the mean thickness of the ice shell and ocean. Though constraints on radial structure are important for understanding the internal dynamics of any planetary body, descriptions of lateral structure additionally allows characterization of processes which create planetary-scale deviation from hydrostatic equilibrium. For example, tidal heating and ocean circulation. Tidal heating and ocean circulation are both expected to result in lateral

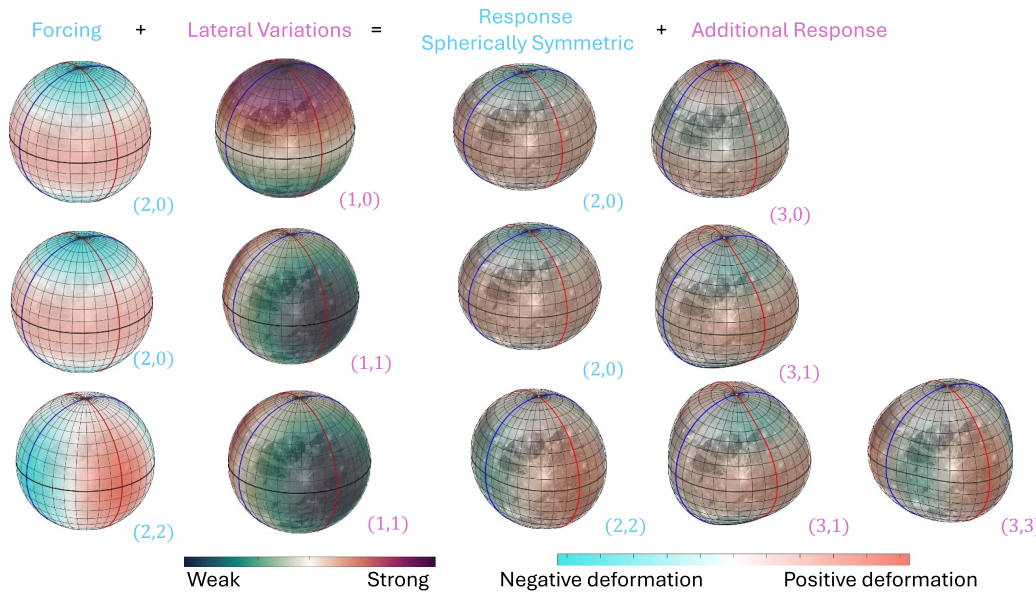

Figure 1. Schematic representation of the tidal response for a body with lateral variations of interior properties. The additional tidal response is expected to be less than 1% of the tidal response, and is exaggerated for visual purposes. Weak regions represent either regions with thinner ice shell or lower shear modulus.

variations in shell thickness (Kang, 2023; Kang & Jansen, 2022; Ojakangas & Stevenson, 1989). Ganymede's surface is characterized by dark and bright regions—with more dark terrain in the leading hemisphere (Patterson et al., 2010)—which might indicate lateral heterogeneity within the shell. Constraining lateral structures will thus provide a window into the moon's dynamics.

Lateral variations in interior properties alter the tidal response of planets and moons (e.g., Berne et al., 2023; Lau et al., 2015; Qin et al., 2014; Rovira-Navarro et al., 2024; Zhong et al., 2012). The wavelength of the tide of a body whose interior properties only depend on radial distance is the same as that of the tidal force. By contrast, if the interior properties also depend on latitude and longitude, the tidal deformation also contains wavelengths different than the wavelength of the forcing. This coupling of tidal modes can be understood by noting that regions with weak mechanical resistance are more prone to deformation under tidal stresses than more rigid regions (see Figure 1).

The additional tidal signal arising from lateral variations can be used to constrain the nature of lateral heterogeneites, a technique known as tidal tomography (Qin et al., 2016; Rovira-Navarro et al., 2024; Zhong et al., 2012). The amplitude of this signal is typically small, nonetheless, tidal tomography has already been used to reveal a deep mantle plume in the Earth (Lau et al., 2017). The dual-frequency X- and Ka-band radio link of the 3GM experiment will provide unprecedented range-rate and range accuracy (Cappuccio et al., 2020). This will not only make it possible to measure the Jovian tide but might also enable the detection of the much weaker moon-moon (e.g., Ganymede-Callisto, Ganymede-Europa) ocean tides (De Marchi et al., 2022; Hay et al., 2022) and potentially the tidal signal associated with the presence of lateral heterogenities within Ganymede. Here, we demonstrate the potential of using tidal tomography to reveal lateral heterogenities within Ganymede.

2. Methods

2.1. Time-Changing Gravity Field and Extended Love Numbers

The gravitational potential ϕ of a body is typically written in terms of spherical harmonic coefficients $\bar{C}_{lm}$ and $\bar{S}_{lm}$

$$\phi(r,\theta,\varphi) = \frac{GM}{r}\sum_{l=0}^{\infty}\sum_{m=0}^{l}\left\{\left(\frac{R}{r}\right)^{l}\bar{P}_{lm}(\cos\theta)\left[\bar{C}_{lm}\cos(m\varphi) + \bar{S}_{lm}\sin(m\varphi)\right]\right\}; \quad (1)$$

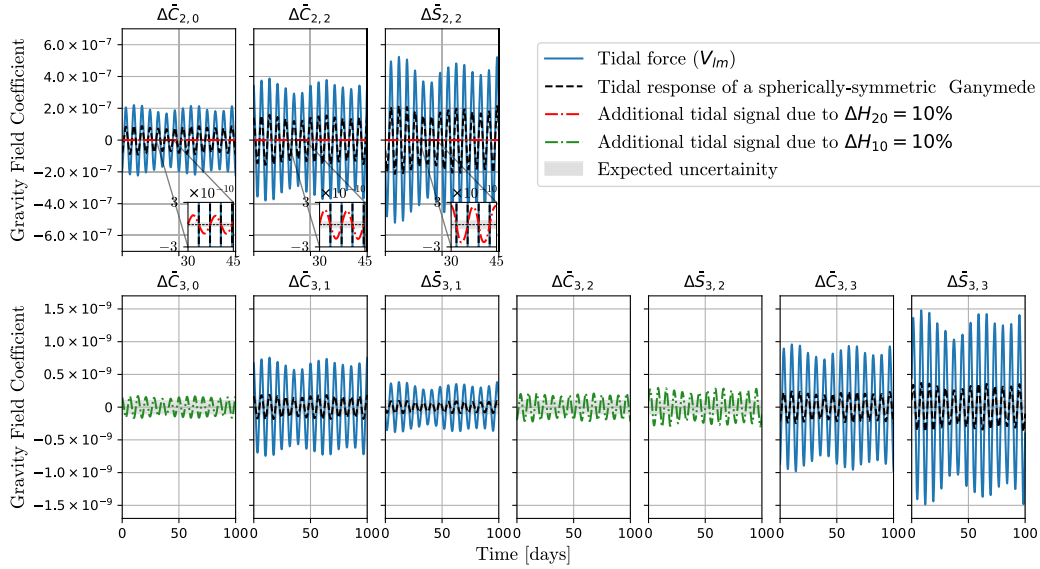

Figure 2. Ganymede's Jovian tide at degree 2 and 3 (V_{lm}) and time-varying components of the gravity field coefficients for a spherically-symmetric Ganymede and one with degree-2 and 1 lateral variations (see Equations 2 and 3). The shaded regions indicate the expected sensitivity of Juice. The computation uses the NOE-5-2021 ephemeris of Ganymede (https://ftp.imcce.fr/pub/ephem/satel/NOE/JUPITER/2021/), which represents an extended analysis of the ephemeris presented by Lainey et al. (2009). The Ganymede rotation model assumes the equator is aligned with the instantaneous orbital plane, and that Ganymede's long-axis (assumed to be aligned with the zero longitude meridian) points to the instantaneous empty focus of the orbit (i.e., no physical libration and obliquity) (Dirkx et al., 2016). The mean values of V_{lm} have been subtracted, since these represent the permanent tide.

where M and R are the mass and the mean volumetric radius of the body; r, θ, and φ the radial distance, co-latitude and longitude where the gravitational potential is evaluated; and $\bar{P}_{lm}$ are the normalized associated Legendre polynomials of degree l and order m.

The gravitational coefficients ($\bar{C}_{lm}$, $\bar{S}_{lm}$) contain both time-independent and a time-dependent components. For synchronous moons with a non-zero eccentricity and obliquity, the latter is mainly caused by tidally-driven deformation at the diurnal period (e.g., 7.1 days for Ganymede). For a spherically-symmetric body, the perturbation to the gravitational field at degree l linearly depends on the forcing at that same degree l, as given by the gravitational Love numbers k_l. Because of this, the effect of tides in the gravitational field is often included as a correction to the gravitational field of the form

$$\Delta \bar{C}_{lm} = k_l \frac{1}{2l+1} \frac{M_j}{M} \left(\frac{R}{d}\right)^{l+1} \bar{P}_{lm}(\theta_j) \cos\left(m\varphi_j\right) = k_l V_{lm} \tag{2a}$$

$$\Delta \bar{S}_{lm} = k_l \frac{1}{2l+1} \frac{M_j}{M} \left(\frac{R}{d}\right)^{l+1} \bar{P}_{lm}(\theta_j) \sin\left(m\varphi_j\right) = k_l V_{l,-m} \tag{2b}$$

with $m \geq 0$ and M_j, φ_j and θ_j being the mass and the longitude and co-latitude of the tide-raising and d the distance from the center of the body to the tide raising body (e.g., Eanes et al., 1983; Konopliv et al., 2013). V_{lm} is the amplitude of the tidal force. Figure 2 shows the degree-2 and 3 time-varying component of Jovian tide at Ganymede during Juice's orbit (V_{lm}) as well as the expected gravity-field changes due to the moon's deformation $\left(\Delta \bar{C}_{lm}, \Delta \bar{S}_{lm}\right)$. Because the scaling of the tidal potential amplitude with degree $\propto (R/d)^{l+1}$, the tidal response is overwhelmingly dominated by degree-two ($l = 2$) terms.

Lateral variations of interior properties induce mode-coupling; a forcing at spherical harmonic degree and order (l, m) can induce a response at degree and order $(l, m') \neq (l, m)$ (Berne et al., 2023; Dahlen & Tromp, 1999; Lau et al., 2015; Rovira-Navarro et al., 2024; Qin et al., 2016). The generalized relationship between forcing and

response can be written in terms of extended Love numbers, $\mathcal{K}_{lm}^{l'm'}$, which relate the response at degree and orders (l', m') to a forcing at degree and order (l, m) (see Text S1 in Supporting Information S1)

$$\Delta \bar{C}_{l'm'} = \sum_{l=2}^{\infty} \sum_{m=0}^{l} \left(\mathcal{K}_{lm}^{l'm'} V_{lm} + \mathcal{K}_{l,-m}^{l'm'} V_{l,-m} \right) \tag{3a}$$

$$\Delta \bar{S}_{l'm'} = \sum_{l=2}^{\infty} \sum_{m=0}^{l} \left(\mathcal{K}_{lm}^{l',-m'} V_{lm} + \mathcal{K}_{l,-m}^{l',-m'} V_{l,-m} \right) \tag{3b}$$

Without lateral heterogeneities, the only non-zero terms are the "diagonal" Love numbers, $l = l'$ and $m = m'$. Moreover, the tidal response does not depend on the order of the tide. When this is the case, we have $\mathcal{K}_{lm}^{lm} = k_l$, reducing Equation 3 to Equation 2.

As evidenced from Equation 3, a laterally heterogeneous body experiences a richer response to forcing than would a spherically symmetric body. The tidal response depends on the forcing order forcing m, and the degree 2 tide can induce a tidal response at higher degrees. As the degree-2 forcing is much larger in amplitude than that at other degrees, $\Delta \bar{C}_{3m}$ might be dominated by the "off-diagonal" Love numbers with $l = 2$ and $l' = 3$ describing the degree-3 response due to degree-2 forcing (see Figure 2).

2.2. Modeling the Tidal Response of a Body With Lateral Heterogeneities

Linking the extended Love number spectra $\left(\mathcal{K}_{lm}^{l'm'}\right)$ to interior properties requires a forward model capable of computing the tides of bodies with lateral heterogeneities. The tides of spherically-symmetric bodies have traditionally been computed using analytical and semi-analytical spectral method based on spherical harmonic functions (Love, 1911; Sabadini et al., 2016). Because of mode-coupling, this computation is more challenging if the body contains lateral heterogenities. Two different approaches have been employed: finite element methods (FEM) (Zhong et al., 2012; A et al., 2014; Berne et al., 2023; Souček et al., 2016, 2019) and spectral methods (Beuthe, 2018; Lau et al., 2017; Qin et al., 2014; Rovira-Navarro et al., 2024). The main advantage of FEM is that they are very versatile. Complicated non-linear relations between stress and strain tensor can be incorporated, making it possible to employ more realistic rheological models and even capture the influence of cracks and faults in the tidal response (Berne et al., 2024; Souček et al., 2024). However, FEMs are typically computationally expensive, limiting these techniques' utility for exploring a wide parameter space and exploiting the power of Bayesian statistics for inversions. In contrast, spectral methods do not have the flexibility typical of FEMs but are much more computationally-efficient and hence more amenable to statistical analysis.

Here, we use the semi-analytical spectral method of Rovira-Navarro et al. (2024) implemented in the LOV3D software package (Rovira-Navarro et al., 2025) (see Text S2 in Supporting Information S1). In LOV3D, lateral variations of interior properties are represented using spherical harmonics. The thickness (H) and elastic shear modulus of a layer (μ) are split into their mean $\left(H_0, \mu_0\right)$ and a laterally-varying component dependent on spherical harmonic degree and order (H_l^m, μ_l^m):

$$(H, \mu) = \left(H_0, \mu_0\right) + \sum_{l,m} \left(H_n^m, \mu_l^m\right) \mathcal{Y}_l^m, \tag{4}$$

where $\mathcal{Y}_l^m$ are real spherical harmonics (Text S1 in Supporting Information S1).

2.3. Ganymede Interior Model

To test the sensitivity of the tidal response to lateral variations, we build a fiducial interior model that includes both radial and lateral variations of interior properties. Our putative Ganymede consists of five layers: a fluid metallic core, a silicate mantle, a high pressure ice layer, a liquid ocean and an outer ice shell (see Table S1 in Supporting Information S1), all consistent with current knowledge of Ganymede (Kamata et al., 2016; Vance et al., 2014, 2018). We neglect the effect of viscoelastic rheology, which is expected to induce a phase-lag (<10deg) in the tide (Hussmann et al., 2016), and focus on the elastic response. Additionally, we assume all internal layers are incompressible. The effect of both of these assumptions is examined below.

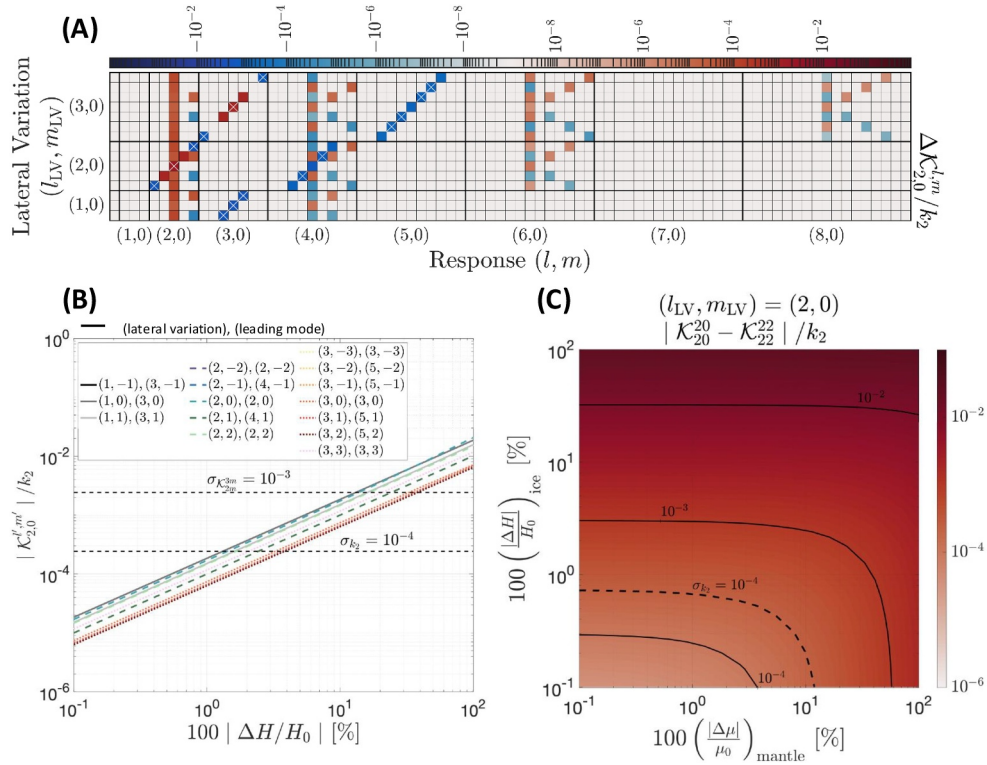

Figure 3. Sensitivity of Ganymede's tidal response to wavelength (a), amplitude (b) and depth (c) of lateral heterogeneities. (a) Shows the Love number spectra arising from 10% shell thickness lateral variations of degree and order (l_{LV}, m_{LV}), the highest term of the tidal response indicated with a cross. The tidal spectra for order 2 and −2 forcing can be found in Figure S1 in Supporting Information S1. (b) Shows the change in amplitude of the leading term with increasing amplitude of lateral variations, the expected uncertainty of Juice's k_2 measurement and the assumed uncertainty in the degree three tidal measurements are indicated with dashed-lines. Due to symmetry, the effect of $\pm m$ lateral variations is the same. Figure S2 in Supporting Information S1 displays the same but for an order 2 forcing. (c) Compares the effect of zonal degree two lateral variations in the ice shell and the deep mantle in the main degree two tidal response. The dashed line indicates Juice's uncertainty. A similar plot but for degree one zonal variations can be found in Figure S4 in Supporting Information S1.

The wavelength and amplitude of potential lateral variations in the Ganymede's ice shell and deep interior are not currently known. Lateral variations in tidal heating in both the shell and deep interior are expected to produce shell thickness variations characterized by degree 2 and 4 and orders 0 $\pm$ 2 and $\pm$4 patterns (Beuthe, 2013; Ojakangas & Stevenson, 1989). Ocean dynamics can similarly produce zonal lateral variations of shell thickness (Kang & Jansen, 2022; Soderlund, 2019). Other processes might also cause ice lateral variations. For instance, Enceladus presents a polar dichotomy in shell thickness of unknown origin (Hemingway & Mittal, 2019; Čadek et al., 2016) and the Moon has a well known nears-side/far-side dichotomy (e.g., Jolliff et al., 2000; Laneuville et al., 2013). We define a fiducial model that contains the patterns expected to dominate tidal heating ($l = 2, m = 0$) and (2,2), as well as polar dichotomy (1,0) and near-side/far-side dichotomy (1,1) (see Figure 4 and Table S2 in Supporting Information S1). The total amplitude of lateral variations is aligned with the plausible range of shell thickness variations estimated by A et al. (2014).

3. Results

3.1. Sensitivity of Ganymede's Response to Lateral Heterogenities

The additional tidal signal arising from lateral heterogenities depends on the geographical distribution, depth and amplitude of such heterogenities. Here, we first explore the effect of lateral structures within the shell and then compare them to the effect of heterogeneities in deeper layers.

The wavelength of lateral variations in internal structure determines the wavelength of the response. For instance, a body with a near-side/far-side dichotomy (i.e., (1,1) lateral variation) under a degree-2 forcing exhibits an

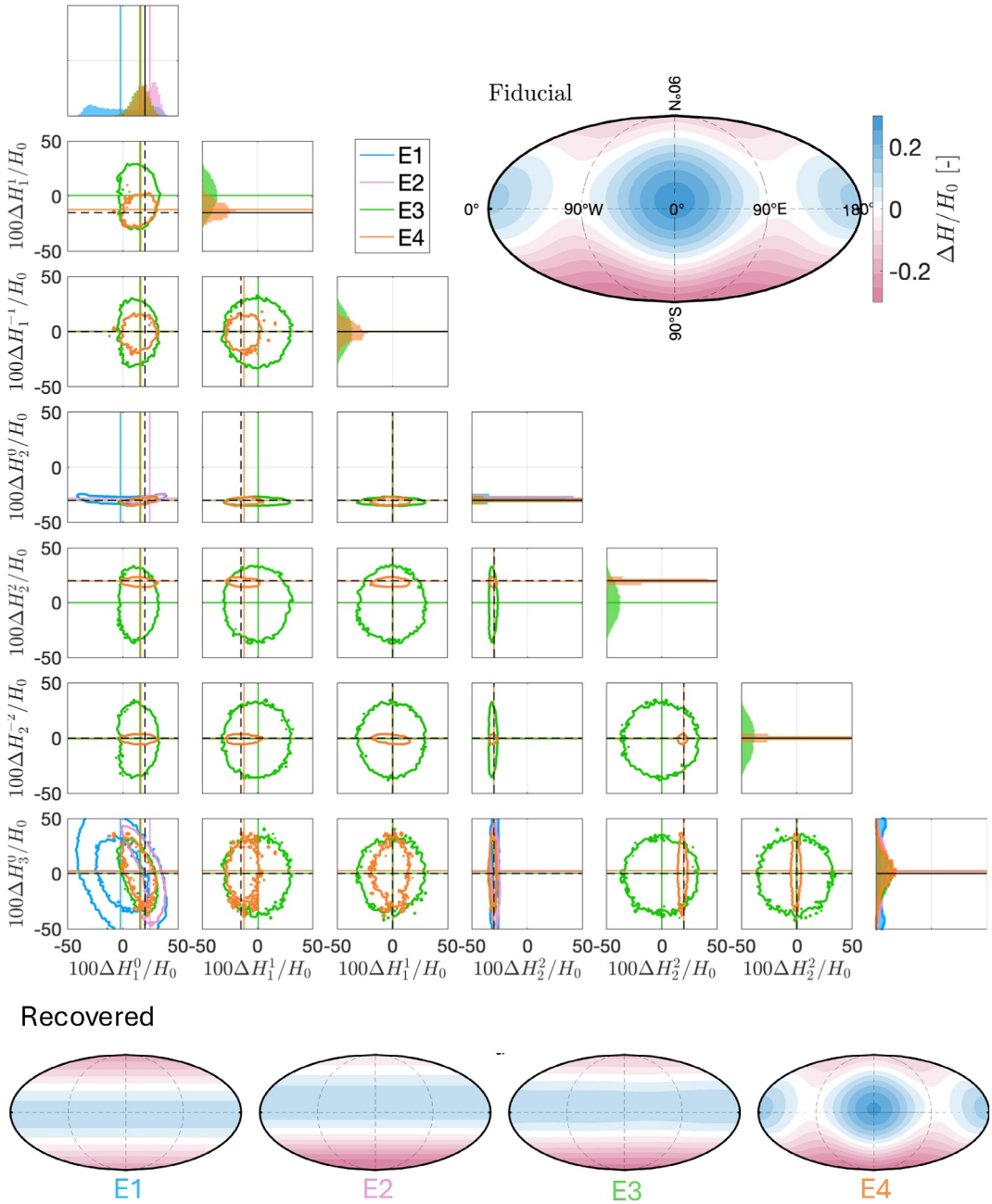

Figure 4. Recovered lateral variations from experiments 1–4 (see Table S3 in Supporting Information S1). The contours correspond to combinations of parameters with a count higher than 5% of the maximum count of said parameters and the black lines indicate the values corresponding to the fiducial model. Maps for the fiducial (upper right) and recovered shell thickness variations for experiments E1–E4 (lower panel) are also given.

additional degree-3 response with a similar hemispherical dichotomy in addition to the typical degree-2 response (see Figure 1). Other types of lateral variations yield a response characterized by other wavelengths. Figure 3a displays the tidal spectra for models with 10% shell thickness variations for geographical patterns of specific spherical harmonic degrees and orders. Each pattern excites unique tidal spectra, yet the amplitude of the tidal components quickly decays as the degree of the response mode increases. In general, the effect of lateral variations depends on the component of the tidal force (see Figures S1 and S2 in Supporting Information S1). For instance, $(l,m) = (2,0)$ lateral variations increase the (2,0) tidal response and decrease the (2,2) response. Such

an effect cannot be mimicked by radial variations in interior properties. Measuring the Love numbers at different orders (e.g., k_{20}, k_{22}), should therefore help distinguish $1D$ structure from potential $3D$ structure.

Degree-1 and 2 lateral variations couple most with the degree 2 tidal forcing (Figure 3b). As expected, the amplitude of the additional tidal response depends on the amplitude of lateral heterogenities (see Figure 3b). The additional signal arising from these terms is of the order of $\sim(10^{-2}\text{-}10^{-3})\cdot k_2$ (with $k_2 = 0.41$) for lateral variations ranging between $\sim 10\% - 100\%$ the mean shell thickness value. If we consider the degree 2 response, this is well above the expected accuracy of the 3GM experiment $\sigma_{k_2} \sim 10^{-4} \sim 2\cdot 10^{-4} k_2$ (Cappuccio et al., 2020). A pole/equator dichotomy (zonal degree two lateral variations) of a few percent produces a signal above this threshold, indicating Juice will be able to detect this kind of lateral structure.

Discerning the accuracy to which Juice can measure higher degree terms, $l > 2$, requires a full covariance analysis of simulated range and range-rate Juice data, akin to that done in De Marchi et al. (2022) for the degree 2 frequency-dependent tidal response but incorporating the new parametrization of the tidal response introduced in Section 2.1. For the degree 3 terms we can get an estimate by using the uncertainty of the degree-three gravity field coefficients, which will be in the order of 10^{-10} (Cappuccio et al., 2020). As shown in Figure 2, this uncertainty is of the same order as the expected time-varying signal arising from a spherically-symmetric Ganymede, $k_3 V_{3m}$. From Equation 3, $\sigma_{K_{2m}^{3m}}$ can be estimated as $\sigma_{K_{2m}^{3m'}} \sim k_3 V_{3m}/V_{2m}$, from which we get $\sigma_{K_{2m}^{3m'}} \sim 10^{-3}$. This uncertainty would imply sensitivity to degree-1 shell thickness variations of $\sim 10\%$ the mean shell thickness (Figures 2 and 3b).

Lateral variations in deeper layers (high pressure ice and mantle) also induce an additional response. The relation between wavelength of lateral variations and the response is the same as for variations in the shell (Figure S3 in Supporting Information S1), however the amplitude is much smaller. To illustrate this point, we consider the sensitivity of the diurnal tide to shear modulus variations in different regions of Ganymede's outer ice shell, high pressure ice, and mantle. We find that Ganymede' time-variable gravity is about 10^2 times more sensitive to structure in the outer ice shell than to heterogenities in the deeper interior (see Figure S5 in Supporting Information S1). For instance, with our reference interior model, producing the same tidal signature of a 3% shell variation requires a 60% variation of mantle shear modulus (Figure 3c). While, deep interior variations of $> 10\%$ are above the detectability threshold, they are not expected—a shear modulus anomaly of $\sim 10\%$ requires a thermal anomaly of ~ 500 K (Isaak, 1992). Moreover, any small variations in shell thickness properties would conceal this signal.

Ganymede's response is also affected by compressibility and viscous effects. A compressible shell with a bulk modulus of 10 GPa yields a tidal Love number $\sim 1\%$ higher than an incompressible shell, roughly the same as that produced by $\sim 50\%$ shell thickness variations and well above the detectability threshold of Juice. However, unlike compressibility effects, shell variations result in a response that is order-dependent (i.e., $k_{20} \neq k_{22}$). Simultaneous measurements of time-variations in the zonal and sectoral components of Ganymede's gravity field should therefore help to distinguish the two effects. $3D$ variations in bulk modulus are expected to be smaller than shell thickness variations and also have a smaller effect on the tidal response than both thickness and shear modulus variations (Qin et al., 2016). Disentangling viscoelastic effects might be more problematic since they can induce a tidal response that appears similar to that produced by $3D$ structure. For example, a $(l,m) = (2,2)$ response induced by (2, 2) structure interacting with the (2, 0) component of the tidal force could be misinterpreted as a phase lag. Here again, careful consideration of the order dependence of the response should allow separation of the two effects, but this requires further investigation.

3.2. Recovering Ganymede Lateral Variations Using a Bayesian Framework

To assess the potential of using tidal tomography to constrain lateral heterogenities, we perform a simulated inversion of internal structure assuming different sets of measurements and uncertainties of gravity field perturbations. We obtain the Love number spectra of the fiducial model of Section 2.3, add Gaussian noise representative of the expected gravity measurements and try to recover the fiducial lateral variations using a Bayesian Markov Chain Monte Carlo inversion with a Metropolis-Hastings sampling algorithm (see Text S3 in Supporting Information S1).

We consider four different experiments in which we vary the number of measured terms of the Love spectra and the complexity of the interior model we try to invert for (see Table S2 in Supporting Information S1). In the first experiment (E1) we assume that only the diagonal Love numbers typically estimated in gravity determination ($\mathcal{K}^{2,0}_{2,0}$, $\mathcal{K}^{2,2}_{2,2}$ and $\mathcal{K}^{2,-2}_{2,-2}$) are measured and try to infer zonal shell thickness variations up to degree 3. In the second (E2), we consider that the degree 3 Love numbers due to forcing at degree 2 arising from zonal lateral variations are also measured (six terms of the Love number spectra also including $\mathcal{K}^{3,0}_{2,0}$ and $\mathcal{K}^{3,2}_{2,2}$). In the third experiment (E3) we also try to obtain sectoral lateral variations up to degree 2 using the same observables as in E2. Finally, in the last experiment (E4), we try to infer zonal (degree 1–3) and sectoral (degree 1–2) using up to 20 terms of the Love number spectra (including degree 2 and 3 terms expected to be excited from sectoral variations) (see Text S2 in Supporting Information S1). From the arguments in the previous section, we set the uncertainty with which Love numbers can be retrieve from Juice tracking data to $\sigma_{\mathcal{K}^{2m'}_{2m}} = 10^{-4}$ and $\sigma_{\mathcal{K}^{3m'}_{2m}} = 10^{-3}$.

In all experiments, we assume the radial profile of interior properties is known. While a joint inversion of $1D$ and $3D$ structure using various types of observations (static gravity and shape, tides, spin-state, radar sounding and magnetic observations) might be desirable, the order dependence of the tidal response for a laterally heterogeneous moon allows to distinguish $3D$ from $1D$ effects. Furthermore, given the small sensitivity to variations in the deep interior, we also only consider lateral variations in shell thickness (Section 3.1), and ignore shear modulus variations in the shell, as the latter are expected to be much smaller and have a smaller effect on the tidal response (A et al., 2014). Moreover, as obliquity tides ($l = 2$ and $m = 1$) are expected to be smaller than eccentricity tides, we focus on the response due to eccentricity tides ($l = 2$ and $m = 0$, $m = \pm 2$) (Chen et al., 2014). These assumptions allow us to isolate the effects of lateral variations and illustrate the potential of using tidal tomography in the simplest set-up. Nonetheless, all stated assumptions may be relaxed in future work or real inversions of data from the 3GM experiment.

The results of the inversion are shown in Figure 4, the recovered values and uncertainties are given in Table S3 in Supporting Information S1 and differences between the fiducial and the recovered model are plotted in Figure S6 in Supporting Information S1. The unprecedented accuracy of the 3GM experiments implies that even if only the degree two response at different orders is measured, as in the nominal 3GM goal, the zonal degree two lateral variations can be recovered with an uncertainty of $\pm 1\%$ (see E1 in Figure 4 and Table S3 in Supporting Information S1).

Measuring off-diagonal terms arising from the degree two forcing allows for extraction of lateral variations with other wavelengths. By measuring changes in the degree 3 gravity field the presence of a polar dichotomy ($l = 1, 3$ and $m = 0$) can be unveiled. Degree 1 lateral variations can be constrained within a $\sim \pm 7\%$ accuracy, while degree 3 lateral can be constrained between a $15\% - 30\%$ accuracy depending on the terms of the tidal spectra measured. Constraining longitudinal variations in shell thickness is more challenging as it requires measuring ~20 different extended Love numbers, but if this is done sectoral lateral variations can be also constrained to less than $\sim \pm 7\%$ accuracy (E3, E4).

4. Summary and Implications

Lateral variations of interior properties induce a coupling between deformation modes of different spherical harmonic degrees and orders. This affects the tidal response of moons and planets, making it possible to constrain lateral structure from very accurate measurements of body tides. We demonstrate that tidal tomography can be used to constrain shell thickness variations in Ganymede. The degree to which this can be done depends on how many extended Love numbers can be extracted from observations. Future work on Juice gravity science should strive to discern how many of these terms can be measured, and de-correlated from other parameters to better-bound their uncertainty. While not explored in this work, recovering $l > 3$ tidal signals would allow to recover shorter wavelength features.

While our work focused on gravity observations, the role of lateral heterogenities might also be detected using altimetry measurements. Future work might explore the sensitivity of GALA measurements to lateral heterogenities, although the lower accuracy of these observations—$\sigma_{h_2} \sim 2 \cdot 10^{-2} h_2$ versus $\sigma_{k_2} \sim 2 \cdot 10^{-4} k_2$ (Steinbrügge et al., 2015)—makes this more challenging. Dynamic gravity and shape data is especially sensitive to long wavelength heterogenities in shallow regions (Figure 3). This technique can complement static shape and gravity

measurements which also have sensitivity at lower spatial scales and deeper structure. Mapping shell thickness would provide insight into different processes relevant for habitability, including the distribution of tidal heating in Ganymede's interior and the global circulation and transport of energy within its subsurface ocean (e.g., Kang & Jansen, 2022; Ojakangas & Stevenson, 1989; Soderlund et al., 2024).

Beyond Ganymede, this work illustrates the power of tidal tomography to detect lateral structures from orbit, presenting an attractive alternative to techniques requiring a lander (e.g., seismology). To exploit this technique, future gravity inversions should move away from the traditional parametrization of tides with diagonal Love numbers $\left(\mathcal{K}_{2m}^{2m}\right)$ to a more general one including off-diagonal Love numbers $\left(\mathcal{K}_{2m}^{l'm'}\right)$ (Section 2.1). The flyby-based trajectory of Europa Clipper makes the independent determination of k_{20}, k_{21}, k_{22} unlikely (Mazarico et al., 2023) but future mission might enable independent observations of these parameters. With icy moon exploration being a top priority for ESA and NASA (National Academies of Sciences et al., 2023; Tacconi et al., 2021), we suggest that tidal tomography be incorporated into the architecture of future missions to the outer solar system.

Data Availability Statement

The software used in this article and which can be used to reproduce the result, LOV3D, is available at Rovira-Navarro et al. (2025).

Acknowledgments
M.R.N. and I.M. were partially supported by the National Aeronautics and Space Administration (NASA) under Grant 80NSSC20K0570 issued through the NASA Solar System Workings program. A.B. is supported by the Future Investigators in NASA Earth and Space Science and Technology Program (80NSSC22K1318). The authors thank Paolo Cappuccio for his helpful comments and insightful discussion about the manuscript.

References

A, G., Wahr, J., & Zhong, S. (2014). The effects of laterally varying icy shell structure on the tidal response of Ganymede and Europa. *Journal of Geophysical Research: Planets*, *119*(3), 659–678. https://doi.org/10.1002/2013JE004570

Berne, A., Simons, M., Keane, J. T., Leonard, E. J., & Park, R. S. (2024). Jet activity on Enceladus linked to tidally driven strike-slip motion along tiger stripes. *Nature Geoscience*, *17*(5), 385–391. https://doi.org/10.1038/s41561-024-01418-0

Berne, A., Simons, M., Keane, J. T., & Park, R. S. (2023). Inferring the mean thickness of the outer ice shell of Enceladus from diurnal crustal deformation. *Journal of Geophysical Research: Planets*, *128*(6), e2022JE007712. https://doi.org/10.1029/2022JE007712

Beuthe, M. (2013). Spatial patterns of tidal heating. *Icarus*, *223*(1), 308–329. https://doi.org/10.1016/j.icarus.2012.11.020

Beuthe, M. (2018). Enceladus' crust as a non-uniform thin shell: I tidal deformations. *Icarus*, *302*, 145–174. https://doi.org/10.1016/j.icarus.2017.11.009

Boutonnet, A., Langevin, Y., & Erd, C. (2024). Designing the JUICE trajectory. *Space Science Reviews*, *220*(6), 67. https://doi.org/10.1007/s11214-024-01093-y

Čadek, O., Tobie, G., Van Hoolst, T., Massé, M., Choblet, G., Lefèvre, A., et al. (2016). Enceladus's internal ocean and ice shell constrained from Cassini gravity, shape, and libration data. *Geophysical Research Letter*, *43*(11), 5653–5660. https://doi.org/10.1002/2016GL068634

Cappuccio, P., Hickey, A., Durante, D., Di Benedetto, M., Iess, L., De Marchi, F., et al. (2020). Ganymede's gravity, tides and rotational state from JUICE's 3GM experiment simulation. *Planetary and Space Science*, *187*, 104902. https://doi.org/10.1016/j.pss.2020.104902

Chen, E., Nimmo, F., & Glatzmaier, G. (2014). Tidal heating in icy satellite oceans. *Icarus*, *229*, 11–30. https://doi.org/10.1016/j.icarus.2013.10.024

Dahlen, F. A., & Tromp, J. (1999). *Theoretical global seismology*. Princeton: Princeton University Press. https://doi.org/10.1515/9780691216157

De Marchi, F., Cappuccio, P., Mitri, G., & Iess, L. (2022). Frequency-dependent Ganymede's tidal Love number k_2 detection by JUICE's 3GM experiment and implications for the subsurface ocean thickness. *Icarus*, *386*, 115150. https://doi.org/10.1016/j.icarus.2022.115150

Dirkx, D., Lainey, V., Gurvits, L., & Visser, P. (2016). Dynamical modelling of the Galilean moons for the JUICE mission. *Planetary and Space Science*, *134*, 82–95. https://doi.org/10.1016/j.pss.2016.10.011

Durante, D., Hemingway, D., Racioppa, P., Iess, L., & Stevenson, D. (2019). Titan's gravity field and interior structure after Cassini. *Icarus*, *326*, 123–132. https://doi.org/10.1016/j.icarus.2019.03.003

Eanes, R., Schutz, B., & Tapley, B. (1983). Earth and ocean tide effects on Lageos and Starlette. In *Proceeding 9th international symposium on earth tides, New York City, August 17-22, 1981* (pp. 239–249).

Goossens, S., Matsuyama, I., Cascioli, G., & Mazarico, E. (2024). A low-viscosity lower Lunar mantle implied by measured monthly and yearly tides. *AGU Advances*, *5*(5), e2024AV001285. https://doi.org/10.1029/2024AV001285

Goossens, S., van Noort, B., Mateo, A., Mazarico, E., & van der Wal, W. (2024). A low-density ocean inside Titan inferred from Cassini data. *Nature Astronomy*, *8*(7), 846–855. https://doi.org/10.1038/s41550-024-02253-4

Grasset, O., Dougherty, M., Coustenis, A., Bunce, E., Erd, C., Titov, D., et al. (2013). JUpiter ICy moons Explorer (JUICE): An ESA mission to orbit Ganymede and to characterise the Jupiter system. *Planetary and Space Science*, *78*, 1–21. https://doi.org/10.1016/j.pss.2012.12.002

Hay, H. C. F. C., Matsuyama, I., & Pappalardo, R. T. (2022). The high-frequency tidal response of ocean worlds: Application to Europa and Ganymede. *Journal of Geophysical Research: Planets*, *127*(5), e07064. https://doi.org/10.1029/2021JE007064

Hemingway, D. J., & Mittal, T. (2019). Enceladus's ice shell structure as a window on internal heat production. *Icarus*, *332*, 111–131. https://doi.org/10.1016/j.icarus.2019.03.011

Hussmann, H., Lingenauber, K., Kallenbach, R., Enya, K., Thomas, N., Lara, L. M., et al. (2019). The Ganymede laser altimeter (GALA): Key objectives, instrument design, and performance. *CEAS Space Journal*, *11*(4), 381–390. https://doi.org/10.1007/s12567-019-00282-8

Hussmann, H., Shoji, D., Steinbrügge, G., Stark, A., & Sohl, F. (2016). Constraints on dissipation in the deep interiors of Ganymede and Europa from tidal phase-lags. *Celestial Mechanics and Dynamical Astronomy*, *126*(1), 131–144. https://doi.org/10.1007/s10569-016-9721-0

Iess, L., Jacobson, R. A., Ducci, M., Stevenson, D. J., Lunine, J. I., Armstrong, J. W., & Tortora, P. (2012). The tides of Titan. *Science*, *337*(6093), 457–459. https://doi.org/10.1126/science.1219631

Isaak, D. G. (1992). High-temperature elasticity of iron-bearing olivines. *Journal of Geophysical Research*, *97*(B2), 1871–1885. https://doi.org/10.1029/91JB02675

Jolliff, B. L., Gaddis, L. R., Ryder, G., Neal, C. R., Shearer, C. K., Elphic, R. C., et al. (2000). New views of the Moon: Improved understanding through data integration. *Eos, Transactions American Geophysical Union*, *81*(31), 349–355. https://doi.org/10.1029/00EO00259

Kamata, S., Kimura, J., Matsumoto, K., Nimmo, F., Kuramoto, K., & Namiki, N. (2016). Tidal deformation of Ganymede: Sensitivity of Love numbers on the interior structure. *Journal of Geophysical Research: Planets*, *121*(7), 1362–1375. https://doi.org/10.1002/2016JE005071

Kang, W. (2023). The modulation effect of ice thickness variations on convection in icy ocean worlds. *Monthly Notices of the Royal Astronomical Society*, *525*(4), 5251–5261. https://doi.org/10.1093/mnras/stad2638

Kang, W., & Jansen, M. (2022). On icy ocean worlds, size controls ice shell geometry. *The Astrophysical Journal*, *935*(2), 103. https://doi.org/10.3847/1538-4357/ac7a32

Kivelson, M., Khurana, K., & Volwerk, M. (2002). The permanent and inductive magnetic moments of Ganymede. *Icarus*, *157*(2), 507–522. https://doi.org/10.1006/icar.2002.6834

Konopliv, A. S., Park, R. S., Yuan, D.-N., Asmar, S. W., Watkins, M. M., Williams, J. G., et al. (2013). The JPL lunar gravity field to spherical harmonic degree 660 from the GRAIL primary mission. *Journal of Geophysical Research: Planets*, *118*(7), 1415–1434. https://doi.org/10.1002/jgre.20097

Konopliv, A. S., & Yoder, C. F. (1996). Venusian k_2 tidal Love number from Magellan and PVO tracking data. *Geophysical Research Letters*, *23*(14), 1857–1860. https://doi.org/10.1029/96GL01589

Lainey, V., Arlot, J.-E., Karatekin, Ö., & Van Hoolst, T. (2009). Strong tidal dissipation in Io and Jupiter from astrometric observations. *Nature*, *459*(7249), 957–959. https://doi.org/10.1038/nature08108

Laneuville, M., Wieczorek, M. A., Breuer, D., & Tosi, N. (2013). Asymmetric thermal evolution of the Moon. *Journal of Geophysical Research: Planets*, *118*(7), 1435–1452. https://doi.org/10.1002/jgre.20103

Lau, H. C. P., Mitrovica, J. X., Davis, J. L., Tromp, J., Yang, H.-Y., & Al-Attar, D. (2017). Tidal tomography constrains Earth's deep-mantle buoyancy. *Nature*, *551*(7680), 321–326. https://doi.org/10.1038/nature24452

Lau, H. C. P., Yang, H.-Y., Tromp, J., Mitrovica, J. X., Latychev, K., & Al-Attar, D. (2015). A normal mode treatment of semi-diurnal body tides on an aspherical, rotating and anelastic. *Earth*, *202*(2), 1392–1406. https://doi.org/10.1093/gji/ggv227

Love, A. (1911). *Some problems of geodynamics*. Cambridge University Press.

Mazarico, E., Buccino, D., Castillo-Rogez, J., Dombard, A. J., Genova, A., Hussmann, H., et al. (2023). The Europa Clipper gravity and radio science. *Investigation*, *219*(4), 30. https://doi.org/10.1007/s11214-023-00972-0

National Academies of Sciences, Engineering, and Medicine. (2023). *Origins, worlds, and life: Planetary science and astrobiology in the next decade*. The National Academies Press. https://doi.org/10.17226/27209

Ojakangas, G. W., & Stevenson, D. J. (1989). Thermal state of an ice shell on Europa. *Icarus*, *81*(2), 220–241. https://doi.org/10.1016/0019-1035(89)90052-3

Padovan, S., Margot, J.-L., Hauck II, S. A., Moore, W. B., & Solomon, S. C. (2014). The tides of Mercury and possible implications for its interior structure. *Journal of Geophysical Research: Planets*, *119*(4), 850–866. https://doi.org/10.1002/2013JE004459

Park, R., Jacobson, R. A., Gomez Casajus, L., Nimmo, F., Ermakov, A. I., Keane, J. T., et al. (2024). Io's tidal response precludes a shallow magma ocean. *Nature*, *638*(8049), 69–73. https://doi.org/10.1038/s41586-024-08442-5

Patterson, G. W., Collins, G. C., Head, J. W., Pappalardo, R. T., Prockter, L. M., Lucchitta, B. K., & Kay, J. P. (2010). Global geological mapping of Ganymede. *Icarus*, *207*(2), 845–867. https://doi.org/10.1016/j.icarus.2009.11.035

Pou, L., Nimmo, F., Rivoldini, A., Khan, A., Bagheri, A., Gray, T., et al. (2022). Tidal constraints on the Martian interior. *Journal of Geophysical Research: Planets*, *127*(11), e2022JE007291. https://doi.org/10.1029/2022JE007291

Qin, C., Zhong, S., & Wahr, J. (2014). A perturbation method and its application: Elastic tidal response of a laterally heterogeneous planet. *Geophysical Journal International*, *199*(2), 631–647. https://doi.org/10.1093/gji/ggu279

Qin, C., Zhong, S., & Wahr, J. (2016). Elastic tidal response of a laterally heterogeneous planet: A complete perturbation formulation. *Geophysical Journal International*, *207*(1), 89–110. https://doi.org/10.1093/gji/ggw257

Rovira-Navarro, M., Matsuyama, I., & Berne, A. (2024). A spectral method to compute the tides of laterally heterogeneous bodies. *The Planetary Science Journal*, *5*(5), 129. https://doi.org/10.3847/PSJ/ad381f

Rovira-Navarro, M., Matsuyama, I., & Veenstra, A. (2025). LOV3D: A spectral method to compute the tides of laterally heterogenous bodies (v2.3) [software]. *Research Data*. 4TU. https://doi.org/10.4121/5511f97f-04b9-479f-9e87-41dc6095a86c.v2

Sabadini, R., Vermeersen, B., & Cambiotti, G. (2016). Global dynamics of the Earth: Applications of viscoelastic relaxation theory to solid-Earth and planetary geophysics: Second edition. Springer. https://doi.org/10.1007/978-94-017-7552-6

Saur, J., Duling, S., Roth, L., Jia, X., Strobel, D. F., Feldman, P. D., et al. (2015). The search for a subsurface ocean in Ganymede with Hubble Space Telescope observations of its auroral ovals. *Journal of Geophysical Research: Space Physics*, *120*(3), 1715–1737. https://doi.org/10.1002/2014JA020778

Soderlund, K. M. (2019). Ocean dynamics of outer solar system satellites. *Geophysical Research Letters*, *46*(15), 8700–8710. https://doi.org/10.1029/2018GL081880

Soderlund, K. M., Rovira-Navarro, M., Le Bars, M., Schmidt, B. E., & Gerkema, T. (2024). The physical oceanography of ice-covered moons. *Annual Review of Marine Science*, *16*(1), 25–53. https://doi.org/10.1146/annurev-marine-040323-101355

Souček, O., Běhounková, M., Čadek, O., Hron, J., Tobie, G., & Choblet, G. (2019). Tidal dissipation in Enceladus' uneven, fractured ice shell. *Icarus*, *328*(100), 218–231. https://doi.org/10.1016/j.icarus.2019.02.012

Souček, O., Běhounková, M., Lanzendörfer, M., Tobie, G., & Choblet, G. (2024). Variations in plume activity reveal the dynamics of water-filled faults on Enceladus. *Nature Communications*, *15*(1), 7405. https://doi.org/10.1038/s41467-024-51677-z

Souček, O., Hron, J., Bêhounková, M., & Čadek, O. (2016). Effect of the tiger stripes on the deformation of Saturn's moon. *Enceladus*, *43*(14), 7417–7423. https://doi.org/10.1002/2016GL069415

Steinbrügge, G., Stark, A., Hussmann, H., Sohl, F., & Oberst, J. (2015). Measuring tidal deformations by laser altimetry. A performance model for the Ganymede Laser Altimeter. *Planetary and Space Science*, *117*, 184–191. https://doi.org/10.1016/j.pss.2015.06.013

Tacconi, L., Arridge, C., Buoanno, A., Cruise, M., Grasset, O., Helimi, A., et al. (2021). *Voyage 2050 final recommendations from the Voyage 2050 senior committee*. European Space Agency. https://www.cosmos.esa.int/web/voyage-2050

Vance, S., Bouffard, M., Choukroun, M., & Sotin, C. (2014). Ganymede's internal structure including thermodynamics of magnesium sulfate oceans in contact with ice. *Planetary and Space Science*, *96*, 62–70. https://doi.org/10.1016/j.pss.2014.03.011

Vance, S., Panning, M. P., Stähler, S., Cammarano, F., Bills, B. G., Tobie, G., et al. (2018). Geophysical investigations of habitability in ice-covered ocean worlds. *Journal of Geophysical Research: Planets*, *123*, 180–205. https://doi.org/10.1002/2017JE005341

Van Hoolst, T., Tobie, G., Vallat, C., Altobelli, N., Bruzzone, L., Cao, H., et al. (2024). Geophysical characterization of the interiors of Ganymede. *Callisto and Europa by ESA's JUpiter ICy moons Explorer*, *220*(5), 54. https://doi.org/10.1007/s11214-024-01085-y

Williams, J. G., Konopliv, A. S., Boggs, D. H., Park, R. S., Yuan, D.-N., Lemoine, F. G., et al. (2014). Lunar interior properties from the GRAIL mission. *Journal of Geophysical Research: Planets*, *119*(7), 1546–1578. https://doi.org/10.1002/2013JE004559

Yoder, C. F., Konopliv, A. S., Yuan, D. N., Standish, E. M., & Folkner, W. M. (2003). Fluid core size of Mars from detection of the solar tide. *Science*, *300*(5617), 299–303. https://doi.org/10.1126/science.1079645

Zhong, S., Qin, C., A, G., & Wahr, J. (2012). Can tidal tomography be used to unravel the long-wavelength structure of the lunar interior? *Geophysical Research Letters*, *39*(15). https://doi.org/10.1029/2012GL052362

References From the Supporting Information

James, R. W., & Cook, A. H. (1976). New tensor spherical harmonics, for application to the partial differential equations of mathematical physics. *Philosophical Transactions of the Royal Society of London. Series A*, *281*(1302), 195–221. https://doi.org/10.1098/rsta.1976.0025

Rovira-Navarro, M., Matsuyama, I., & Hay, H. C. F. C. (2023). Thin-shell tidal dynamics of ocean worlds. *The Planetary Science Journal*, *4*(2), 23. https://doi.org/10.3847/PSJ/acae9a